

Article

Enhanced Photo-Catalytic Performance of Activated Carbon Fibers for Water Treatment

Konstantinos V. Plakas ^{1,*}, Athina Taxintari ² and Anastasios J. Karabelas ¹

¹ Chemical Process and Energy Resources Institute, Centre for Research and Technology Hellas (CERTH), 6th km Charilaou-Thermi Road, Thermi, 57001 Thessaloniki, Greece

² Department of Physics, University of Ioannina, 45110 Ioannina, Greece

* Correspondence: kplakas@cperi.certh.gr; Tel.: +30-2310-498-476

Received: 28 July 2019; Accepted: 28 August 2019; Published: 29 August 2019



Abstract: The synthesis, characterization, and performance of composite photocatalytic adsorbents are investigated in this work using the dip-coating and the electrophoretic coating methods for the deposition of titanium dioxide (TiO₂) on porous activated carbon fiber (ACF) substrates. The adsorption and photocatalytic efficiency of the synthesized catalytic adsorbents were compared using phenol as the model pollutant. Both immobilization techniques resulted in composite ACF/TiO₂ adsorbents characterized by large surface area ($844.67 \pm 45.58 \text{ m}^2 \text{ g}^{-1}$), uniform distribution of TiO₂ nanoparticles on the activated carbon fibers, and high phenol adsorption. The method and the treatment time affected the phenol adsorption, while the highest sorption was determined in the case of the ACF/TiO₂ sample prepared by the electrophoretic coating method (at 20 V) for an electrolysis time of 120 s ($7.93 \text{ mg}_{\text{phenol}} \text{ g}^{-1} \text{ ACF/TiO}_2$). The UV-A irradiation of most ACF/TiO₂ samples led to a faster removal of phenol from water as a result of the combined sorption and heterogeneous photocatalysis. The stability and the effective regeneration of the most promising composite photocatalytic adsorbent was proved by multiple filtration and UV-A irradiation cycles.

Keywords: activated carbon fiber; titanium dioxide; electrophoresis; dip-coating; photocatalysis; adsorption; phenol

1. Introduction

In the last two decades, intensive research activity has been ongoing toward the development of so-called advanced oxidation processes (AOPs) as effective and environmentally friendly methods for disinfection, chemical detoxification, and removal of taste and odor compounds in water and wastewater [1–3]. The remarkable efficiency of AOPs is based on the generation of highly reactive hydroxyl radicals ($\bullet\text{OH}$) that are powerful, non-selective, oxidizing species, which can indiscriminately degrade organic pollutants until their mineralization leads to CO₂, H₂O, and, eventually, inorganic ions as final products [4]. AOPs have the advantage of being environmentally-friendly, as they neither transfer pollutants from one phase to the other (as in chemical precipitation and volatilization), nor produce massive amounts of hazardous side-streams [5]. In comparison to chemical and biological processes, AOPs operate at near ambient conditions, are less energy-demanding, and do not require special installations [6]. The growing interest of academic and industrial communities in AOPs is reflected in the increasing number of publications in several peer-reviewed journals, patents, and international conferences dedicated to the environmental applications of AOPs. For example, over 7000 articles have been published in journals of the Science Citation Index in the last five years dealing with processes such as photocatalysis, ozonation, Fenton reactions, electrochemical processes, wet air oxidation, and ultrasonic cavitation; about 25% of them are devoted to photocatalytic processes. AOPs can provide effective technological solutions for water treatment, thus supporting and

enhancing the competitiveness of different industrial sectors, including the water technology sector in the global market.

The most popular technique among AOPs is the heterogeneous photocatalysis, where a semiconductor photocatalyst interacts with light of sufficient energy (or of a certain wavelength) to produce reactive oxidizing species, which can lead to the photocatalytic degradation of pollutants [7]. Large scale application of heterogeneous photocatalysis may be constrained, however, by technical challenges mainly related to the effective recovery and extended use of the catalyst particles in a continuous process [8,9]. An alternative promising approach is the immobilization of photocatalysts on porous adsorbents, such as carbon, clays, zeolite, and others, which offer the synergistic combination of adsorption and catalytic degradation of the adsorbed pollutants by UV/visible light irradiation. Such an approach allows continuous reuse of the photocatalyst and improved removal of pollutants from water [10].

Activated carbon fibers (ACFs) are microporous carbon materials that present uniform pore size distribution, larger surface area, and faster adsorption rates than other activated carbons, such as granular and powdered [11]. Moreover, ACFs can be made in various forms, such as yarn, thread, fabric, and felt, making them suitable for various applications [12]. These features justify the selection of ACFs as a potential substrate for the successful immobilization of catalytic particles, semiconducting metal oxides in particular, for photocatalytic and photoelectrochemical applications [13,14]. The high adsorption capacity of ACFs, and of carbon-based supporting materials in general, helps form a high concentration environment of adsorbates around the catalytic particles, resulting in an increase in the photo-degradation rate [15]. Among the many different photocatalysts proposed in literature, titanium dioxide (TiO_2) has been the most widely studied and used in many applications because of its greater photocatalytic activity compared to other semiconductors, its long-term stability and durability under extreme conditions (pH, temperature, ultraviolet radiation, high shear stresses), and its high resistance to chemical and photodegradation, that all favor its recycling and reuse. Moreover, TiO_2 is superhydrophilic, biologically inactive, environmentally friendly, inexpensive, and commercially available [16].

The immobilization of TiO_2 on porous substrates has been investigated by different methods, such as sol-gel, dip-coating from suspension, electrophoretic coating, hydrothermal, etc. [17]. Table 1 lists representative works of composite TiO_2 adsorbents employing as substrates, specifically carbon-based materials in the form of fibers. Most research groups applied the dip-coating method for TiO_2 immobilization onto carbon fabrics, usually followed by calcination at elevated temperatures (varying from 300 to 750 °C) in argon or nitrogen atmosphere to obtain highly crystalline TiO_2 . A TiO_2 sol was applied in most studies using tetrabutyl orthotitanate ($\text{Ti}(\text{OBu})_4$) as the titanium precursor and ethanol as the solvent. The gradual evaporation of ethanol resulted in $\text{Ti}(\text{OBu})_4$ hydrolysis into anatase TiO_2 with the water vapor in the moist environment. Only a few studies used mixed-phase TiO_2 catalysts for this purpose, such as the commercially available Degussa P25 TiO_2 nanoparticles (25% rutile and 75% anatase according to the manufacturer) [18], although this has been proven as the leading semiconductor photocatalyst for the degradation of a multitude of refractory organic contaminants [19,20]. This trend is probably due to the distinct features of anatase, such as the lower rates of recombination [21] and higher surface adsorptive capacity [22] that renders it the most photochemically active phase of titania. Photocatalytic studies with composite catalytic adsorbents show, in general, high degradation rates of contaminants, which greatly vary depending on the immobilization method, the properties of the porous adsorbent (i.e., specific surface area, pore volume, pore size distribution), and the treatment conditions (initial solution pH, radiation intensity, TiO_2 loading).

A promising alternative to the dip-coating/sol-gel method is the electrophoretic coating method, which has been proven to be a simple and effective method for obtaining reproducible and highly active photocatalytic materials [23]. In a recent work by Pereira et al. [24], TiO_2 electrodeposition on both carbon fiber and boron doped diamond/carbon fiber substrates using TiO_2 sol as the titanium precursor

led to controlled anatase formation and to the production of electrodes with different photocatalytic activities that were largely affected by the TiO₂ deposition time (increased thickness and homogeneity with time) and the nature of the substrate. Motivated by the promising attributes of electrophoresis (i.e., easy method employing simple potentiostatic electrolysis and post-heating at low temperatures, synthesis of reproducible, recyclable, and high photocatalytic activity adsorbents), the present work investigates the adsorptive and photocatalytic activity of ACF/TiO₂ composites prepared by the electrophoretic coating method using phenol as the model organic pollutant. For comparison, ACF/TiO₂ composites are also prepared according to a dip-coating method using titanium (IV) isopropoxide and Degussa P25 as the titanium source. The effect of coating time and the source of titanium dioxide on the surface and structural characteristics of the composite fiber materials are systematically investigated.

Table 1. Methods of TiO₂ immobilization on carbon fiber substrates.

Method	Substrate	Results	Ref.
Sol-gel adsorption	Commercial activated carbon fiber	Calcination temperature greatly affected the structure morphologies of TiO ₂ films; rapid removal of Methyl Orange and acid fuchsine	[25]
Dip-coating	Viscose rayon-based carbon fibers (activated carbon fiber)	Photocatalytic degradation of Methyl Orange and phenol described by first-order kinetics; effective reuse of the activated carbon fiber (ACF)-supported photocatalyst	[26]
Dip-coating	Polyacrylonitrile carbon fiber (modified with Pd)	TiO ₂ /Pd-carbon fiber (CF) exhibited 70% higher catalytic efficiency for Acid Orange II removal than TiO ₂ /CF	[27]
In-situ deposition	Commercial carbon fiber	Fabricated three-dimensional electrode composed of dendritic Ag@Pt core-shell catalyst, reduced graphene oxide, TiO ₂ spheres, and carbon fiber exhibited improved photo-electrocatalytic performance for methanol oxidation compared to other comparative electrodes	[28]
Mixing with Ti(OH) ₄ and H ₂ O ₂	Commercial carbon fiber	The photocatalytic degradation of Methyl Orange found to be phase composition-dependent and pH dependent	[29]
Dip-coating and annealing under superheated steam	Polyacrylonitrile carbon fiber	TiO ₂ /CF composites achieved up to 98.7% degradation rate of Acid Orange II after 2.5 h of irradiation	[30]
Hydrothermal	Commercial activated carbon fiber	The composite ACF/TiO ₂ presented good uniformity, high crystallinity, and large benzene photo-oxidation and sorption affinity	[14]
Ultra-sonication induced adsorption or electrospinning	Polyacrylonitrile nanofiber	TiO ₂ nanoparticles decorated carbon nanofibers, prepared by ultra-sonication, presented higher Methylene Blue adsorption capacity and photo-catalytic efficiency than those obtained by electrospinning	[18]

2. Materials and Methods

2.1. Materials

Activated carbon fibers (ACFs) in felt form, supplied by SO-EN Co. Ltd. (Takasaki, Japan) (code number ACFNW-EM3), were used in this study as substrate for the immobilization of TiO₂. ACF specimens were cut into disks of ~59 mm diameter and pretreated before use (Table 2). All ACF specimens were weighted before and after the immobilization of TiO₂ for assessing the loading of catalyst on the adsorbent surface. Titanium (IV) isopropoxide (TTIP), purchased from Aldrich (≥97%, Steinheim, Gemrnay), and Aeroxide® P-25 (Degussa-Evonik, Frankfurt, Germany) were used as

titanium precursors. High purity Milli-Q water (resistivity 18.2 M Ω , Millipore, Milford, MA, USA), concentrated solutions of nitric acid (65% w/w, Chemlab NV, Steinheim, Germany), and sulfuric acid (95%–97% w/v, Sigma-Aldrich, Steinheim, Germany) were used for the preparation of the composite ACF/TiO₂ adsorbents. Photocatalytic degradation studies were performed with aqueous solutions of phenol ($\geq 99\%$, Sigma-Aldrich, Steinheim, Germany) at 10 mg L⁻¹ in deionized water.

Table 2. Protocol of TiO₂ immobilization on ACF according to electrophoretic coating and dip-coating methods.

ACF Pretreatment	Electrolysis of ACF specimens at a fixed potential of 2.0 V/Ag/AgCl for 30 min in a 0.5 mol L ⁻¹ H ₂ SO ₄ solution followed by overnight drying at 105 °C
TiO ₂ sol Preparation	<ol style="list-style-type: none"> 1. <i>TTIP in Milli-Q water</i> (a) Addition of 36 mL titanium (IV) isopropoxide (TTIP) and 3.8 mL HNO₃ solution in 400 mL Milli-Q water, (b) gentle stirring for 24 h, (c) heating of the homogeneous solution at 55 °C for 6 h 2. <i>Degussa P-25 in Milli-Q water</i> (a) Addition of 9.71 gr TiO₂ in 400 mL Milli-Q water, (b) sonication for 30 min 3. <i>Degussa P-25 in methanol</i> (a) Addition of 50 mg TiO₂ in 500 mL methanol, (b) sonication for 15 min
TiO ₂ Immobilization	<ol style="list-style-type: none"> 1. <i>Dip-coating</i> Dipping of ACF specimens in TTIP solution varying the deposition time: (a) 10 s (ACF-TTIP-10), (b) 30 s (ACF-TTIP-30), (c) 60 s (ACF-TTIP-60) Dipping of ACF specimen in Degussa P-25 suspension varying the deposition time: (a) 10 s (ACF-P25-10), (b) 30 s (ACF-P25-30), (c) 60 s (ACF-P25-60) 2. <i>Electrophoretic coating</i> Electrolysis of methanol Degussa P-25 solution under potentiostatic mode at a fixed potential of 10 V/Ag/AgCl varying the electro-deposition (EDP) time: (a) 30 s (ACF-EDP-30), (b) 60 s (ACF-EDP-60), (c) 120 s (ACF-EDP-120)
ACF/TiO ₂ Post-Treatment	Heating at 200 °C for 5 h and storage in desiccator at room temperature for further use

2.2. Preparation of ACF/TiO₂ Composite Adsorbents

Table 2 summarizes the immobilization protocol and the respective conditions applied for each of the two TiO₂ coating methods investigated in this work. The pretreatment and the electrophoretic deposition were carried out at room temperature using a VersaSTAT3 potentiostat/galvanostat (Princeton Applied Research, AMETEK, Oak Ridge, TN, USA), connected to a PC for continuous monitoring of cell current (VersaStudio software, V3-200, Oak Ridge, TN, USA). These operations were performed in a transparent three-electrode Plexiglas cell using a stainless steel rod as a counter electrode and an Ag/AgCl electrode ($E = 0.207$ V vs SHE) from Metrohm as the reference electrode. Electrolysis was applied for the pretreatment of all ACF specimens, aiming to oxidize them and impart some hydrophilicity as ACFs are highly hydrophobic.

2.3. Characterization

The surface area and pore volume of the samples were measured by nitrogen adsorption-desorption with a TriStar 3000 porosimeter (Micromeritics, Norcross, GA, USA). The specific surface area (A) of the electrodes was measured at liquid nitrogen temperature (77 K), using the Brunauer–Emmett–Teller (BET) method in the relative pressure (P/P_0) range of 0.005–0.50. The morphologies of the composite ACF/TiO₂ adsorbents and the original ACF were examined using a JSM6300 microscope (JEOL, Peabody, MA, USA) equipped with an X-ray Microanalysis–Energy Dispersive Spectroscopy (EDS), operating at 20 kV. The samples were gold sputtered to avoid charging effects on the images.

2.4. Adsorption and Photocatalytic Degradation Studies

Adsorption and photocatalytic degradation tests were performed in a magnetically stirred closed cylindrical vessel made of transparent Plexiglas (>90% transmittance at wavelengths >320 nm) of 600 mL volume. ACF and ACF/TiO₂ specimens were placed in a special Teflon plate (outer/inner diameter 60/51 mm) and immersed in the vessel at a close distance to the wall. For the scope of the electrophoretic deposition, a stainless steel ring was also placed in the Teflon plate in contact with the ACF and used as a charge carrier (connection to the potentiostat by means of a Cr/Ni wire). Photocatalytic experiments were conducted using a low pressure ultraviolet mercury lamp (Blacklight, 365 nm, 5 W) placed outside the Plexiglas vessel at a distance of 2–3 cm from the Teflon plate (and the ACF/TiO₂ adsorbent). Samples were collected from the vessel at certain time intervals for determining residual phenol concentration using a UV–vis spectrophotometer (Spectroquant® Pharo 300, Merck, Darmstadt, Germany) at 270 nm. Measurements of the UV–Vis spectra of samples were also performed, in the range 190–390 nm, for the qualitative assessment of the oxidative reactions taking place in the phenol solution. It is noted that all experiments were conducted in duplicate, and the averaged measured values are reported in this study. The variation was estimated to be within ±8% and ±14% for the adsorption and photocatalysis experiments, respectively.

3. Results and Discussion

3.1. Characterization of ACF/TiO₂ Composite Adsorbents

Figure 1 shows SEM photomicrographs of the ACF specimens before and after the immobilization of TiO₂ nanostructures on their surface. According to Figure 1a, the original ACF consists of unidirectional bundles of pure carbon fibers of about 12 μm in diameter. Figure 1b–d indicate that all ACF fibers were covered by TiO₂ nanostructures of different size and morphology depending on the applied coating method and the deposition time. The presence of Ti on the outer surface of the fibers is also confirmed by the corresponding EDS analyses, according to which the characteristic Ti peaks at 4.6 and 4.95 keV appear only in the modified fibers.

As expected, the dip-coating method resulted in compact and large TiO₂ agglomerates on the fiber surface (Figure 1b,c). This is particularly evident in the case of TTIP rather than in Degussa P-25. Specifically, the use of TTIP as a titanium precursor led to the formation of uniform aggregates with increased thickness at longer deposition times. In contrast, Degussa P-25 displayed irregular structures of TiO₂ crystals, which were unevenly distributed on the outer surfaces of the fibers. The electrophoretic method promoted the uniform distribution of small spherical TiO₂ nanoparticles on the fiber surface (Figure 1d), which can contribute to a better and more stable photocatalytic performance, as discussed next.

The porous structure of the ACF was not significantly altered by the deposited TiO₂ nanoparticles, regardless of the immobilization method and the source of the used titania. As shown in Table 3, specific surface area and average pore volume were reduced by ~29.4%, 24.4% and 1.2% in the case of the ACF-TTIP, ACF-P25, and ACF-EDP samples, indicating that the pores of the ACF were moderately blocked by the loaded TiO₂. In the case of electrophoresis, the deposition of TiO₂ had negligible effect on the surface characteristics of ACF fibers, with the highest electrophoretic coating time (120 s) leading to improved specific surface area and mean pore volume (Table 3). Obviously, some TiO₂ nanoparticles are squeezed to the fiber surface, thereby increasing the surface roughness and the specific surface area.

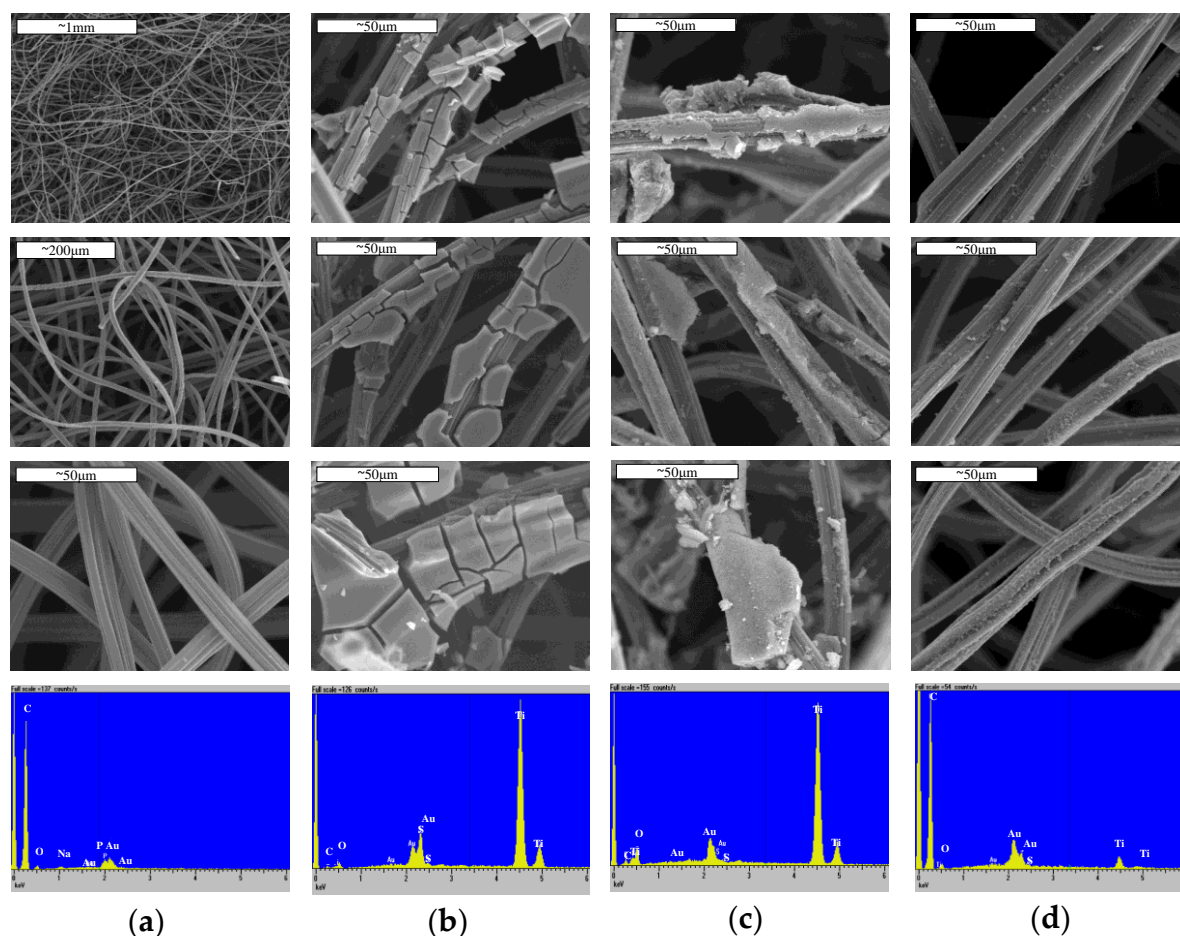


Figure 1. SEM photomicrographs and EDS analysis results of (a) the original ACF at different resolution values, (b) ACF/TiO₂ photocatalytic adsorbents prepared by the dip-coating method in TTIP sol at 10, 30, and 60 s deposition times; EDS analysis of ACF-TTIP-60, (c) ACF/TiO₂ photocatalytic adsorbents prepared by the dip-coating method in Degussa P-25 sol at 10, 30, and 60 s deposition times; EDS analysis of ACF-P25-60, (d) ACF/TiO₂ photocatalytic adsorbents prepared by the electrophoretic coating method with Degussa P-25 sol at 30, 60, and 120 s deposition times; EDS analysis of ACF-EDP-120 (Table 1).

Table 3. Results of Brunauer–Emmett–Teller (BET) analysis and phenol adsorption testing with original ACF and ACF/TiO₂ composites (Table 1).

Sample	BET Specific Surface Area (m ² g ⁻¹)	Mean Pore Volume (cm ³ g ⁻¹)	Phenol Adsorbed (mg _{Phenol} g _{adsorbent} ⁻¹)
ACF	1155.29 ± 4.93	265.39	10.16
ACF-TTIP-10	852.99 ± 3.41	195.95	6.20
ACF-TTIP-30	868.70 ± 3.77	199.56	5.59
ACF-TTIP-60	726.67 ± 2.70	166.93	5.45
ACF-P25-10	890.26 ± 3.40	204.51	3.49
ACF-P25-30	856.69 ± 3.83	196.80	5.78
ACF-P25-60	872.72 ± 3.43	200.48	5.47
ACF-EDP-30	1123.54 ± 5.48	258.10	6.94
ACF-EDP-60	1121.16 ± 4.90	257.55	6.82
ACF-EDP-120	1180.70 ± 5.59	271.22	7.93

3.2. Phenol Adsorption on Original ACF and ACF/TiO₂ Composites

Figure 2 shows the results of preliminary adsorption tests performed with the unmodified ACF. A rather rapid adsorption is observed, and the experimental data are best correlated by pseudo-second-order reaction kinetics (Figure 2a, inset). This implies that the occupation rate of adsorption sites is proportional to the square of the number of unoccupied sites. The values of adsorption constants and correlation coefficients obtained for two well-known adsorption models (Freundlich and Langmuir) are presented in the inset of Figure 2b. The adsorption isotherms were obtained by fitting the adsorbed amounts of phenol on the ACF surface (in units $\text{mg}_{\text{Phenol}} \text{g}_{\text{ACF}}^{-1}$) and the equilibrium phenol concentration ($[\text{Phenol}]_e$) in aqueous solutions (Figure 2b). The Langmuir isotherm seems to fit better the results of phenol adsorption on ACF ($R^2 = 0.958$), implying that a monolayer adsorption takes place on the energetically homogeneous ACF surface, with no transmigration of adsorbate molecules in the plane of the surface. The driving forces for adsorption of phenol probably originate from physisorption based on hydrophobic π - π interactions between the carbonaceous surface and the aromatic ring of the phenol molecules. Chemisorption of phenol molecules due to the interaction with the edges of the basal planes in the carbon fibers is also possible.

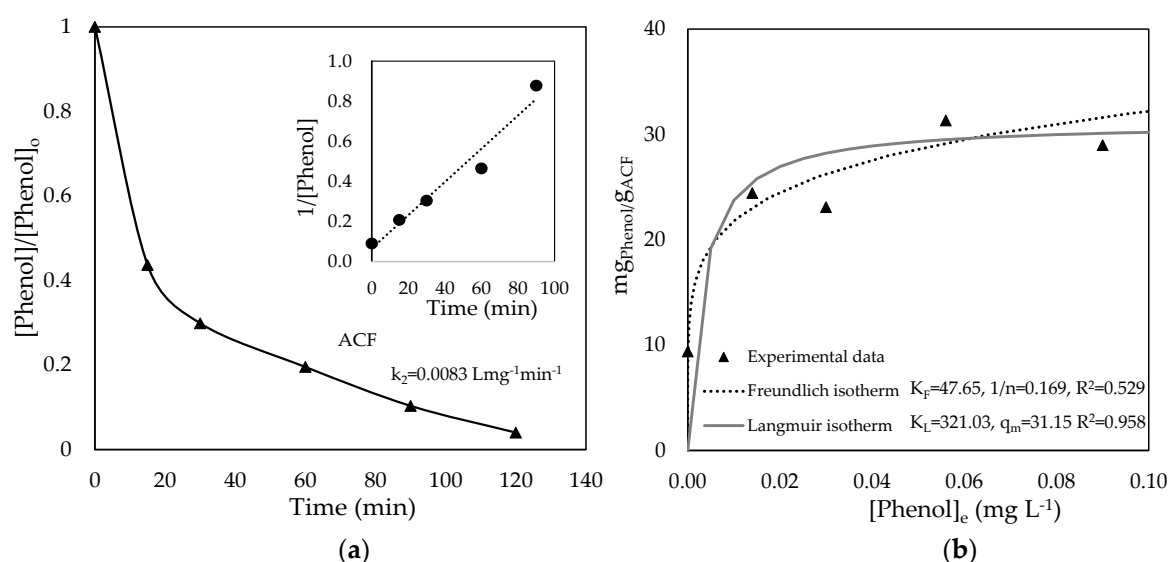


Figure 2. (a) Kinetics of phenol adsorption on the unmodified ACF (inset: second-order kinetics graph and respective rate constant), (b) non-linear fitting of Freundlich and Langmuir isotherm models for ACF adsorbent.

The adsorption rates of phenol molecules on the nine prepared ACF/TiO₂ composite adsorbents are shown in Figure 3. The respective pseudo-second-order reaction kinetics data, also shown in the inset of Figure 3, indicate that adsorption performance is in the following order: ACF-TTIP-10 > ACF-EDP-30 > ACF-TTIP-30 > ACF-EDP-60 > ACF-EDP-120 > ACF-TTIP-60 = ACF-P25-30 = ACF-P25-60 > ACF-P25-10. In comparison to the original ACF (Figure 2a), the kinetic constants significantly decreased from 47% to 93%. However, the respective amounts of phenol adsorbed per unit mass of ACF/TiO₂ adsorbent (at the pseudo-equilibrium time of 120 min) were lower, varying from 21.9% to 65.6% (Table 3). This difference may be attributed to the mass loss of the composite fibers (smaller denominator) due to their electrolytic and thermal pre-oxidation. Based on the experimental data, the adsorption capacity differed between the composite adsorbents, depending on the method and the coating time applied, being greater in the case of adsorbents prepared by the electrophoretic method. According to Table 3, such an adsorption performance is justified by the high specific surface area of the ACF-EDP composites, especially of the one prepared for 120 s of electrodeposition.

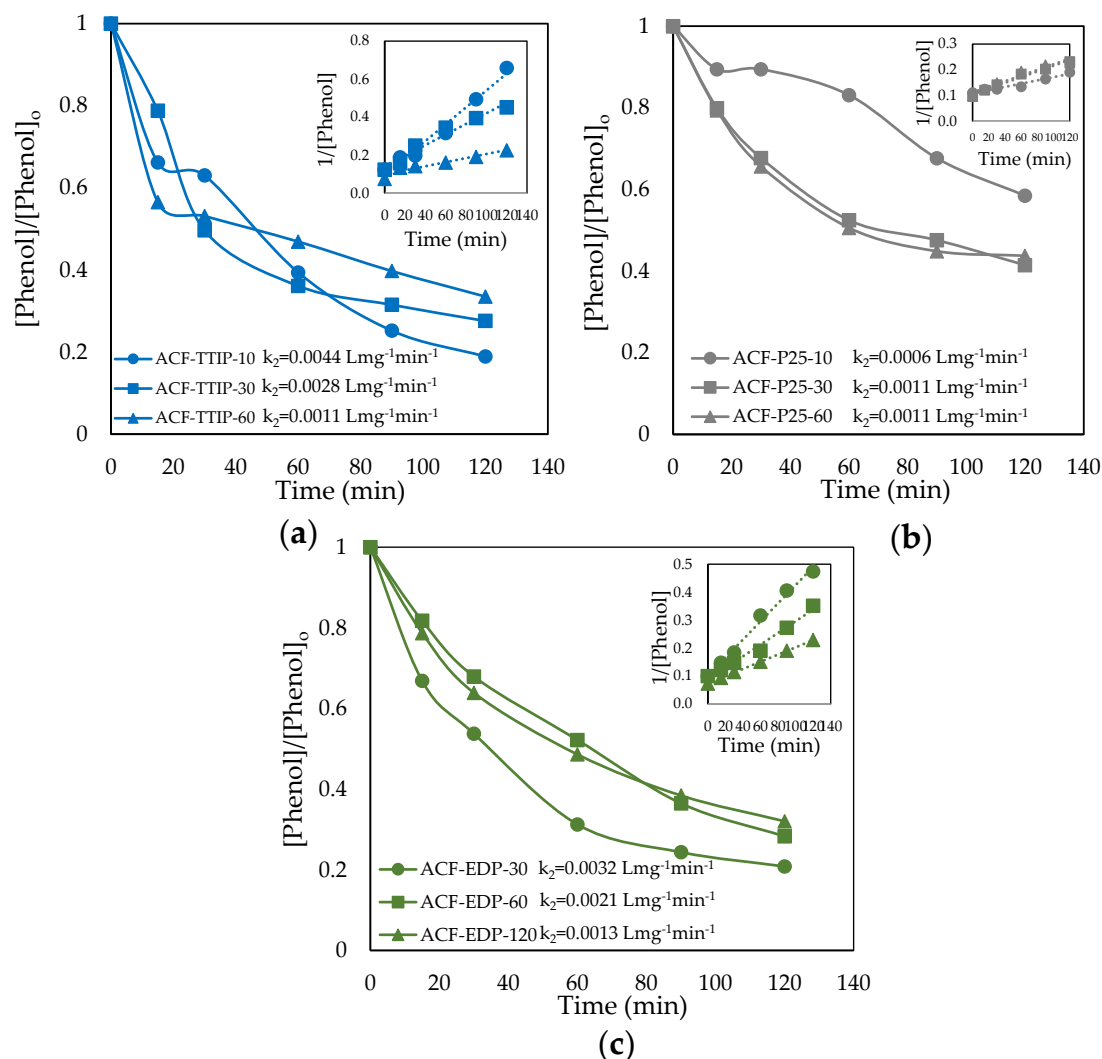


Figure 3. Kinetics of phenol adsorption on (a) ACF-TTIP, (b) ACF-P25, and (c) ACF-EDP composite ACF/TiO₂ adsorbents (inset: second-order kinetic graphs and respective rate constants).

3.3. Phenol Photocatalytic Degradation by ACF/TiO₂ Composites

The results of the photocatalytic degradation tests with the ACF/TiO₂ composites are summarized in Figure 4. In the same Figure, the results are compared with those corresponding to phenol adsorption on unmodified ACF and ACF/TiO₂ composites. A reference photolysis test in the absence of carbon fibers was also performed, showing the limited effect of UV-A irradiation on phenol degradation (14.3% removal). This was expected, since the blacklight lamp used emits at 365 nm, which is far from the maximum UV absorption of phenol (270 nm). In comparison to the simple adsorption tests, the respective photocatalytic experiments resulted in improved removal efficiencies for most of the composite ACF/TiO₂ adsorbents tested due to the combined effects of adsorption and photocatalysis. Specifically, seven out of the nine composites exhibited significantly improved performance, which varied from approximately 85% to 93%. A decline in phenol removal efficiency was observed only in the case of the ACF-TTIP and ACF-P25 samples, prepared at low deposition times (10 s), for which phenol removal decreased by 18.9% and 42.2%, respectively. In contrast, the lower deposition time (30 s) in the case of the ACF-EDP composite led to the best results, with the percentage removal of phenol (~93%) being close to that measured for the adsorption on the unmodified ACF (~96%). These results clearly demonstrate the significant effect of the TiO₂ immobilization method and the coating/deposition time on process performance. The electrophoretic method proves to be the most effective, followed by the dip-coating method with TTIP as the titanium precursor. Regarding the

coating time, different effects were observed between the two methods; i.e., an increase in contact time was beneficial only for the synthesis of ACF-TTIP composites.

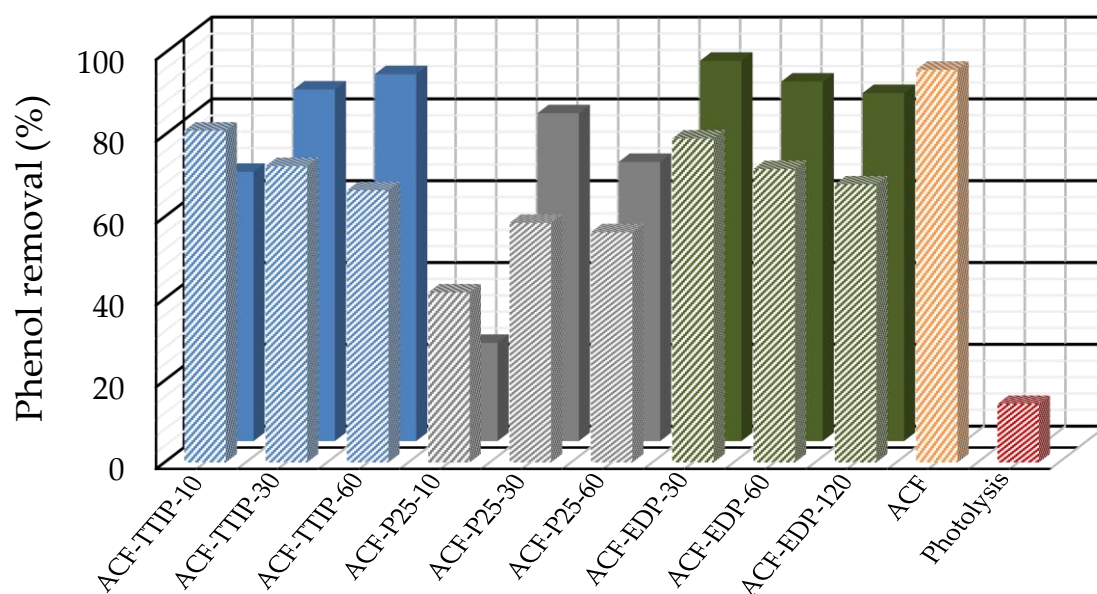


Figure 4. Percentage removal of phenol by the prepared ACF/TiO₂ composite adsorbents due to adsorption (shaded blocks) and combination of adsorption with photocatalysis (solid blocks).

The improved performance of the composite ACF/TiO₂ adsorbents is linked with their three-dimensional structure, which favors both the binding of phenol molecules on the surface of activated carbon fibers and their degradation by the strong hydroxyl radicals ($\bullet\text{OH}$) generated by the diffused ultraviolet radiation on the immobilized photocatalyst (TiO₂). The radicals can interact both with the adsorbed phenol molecules and those dissolved molecules close to the surface of the photocatalyst. Other potential enhancement mechanisms may be involved in the separation of photo-generated electron-hole pairs and in reducing the recombination by the formation of interfacial heterojunction [31]. Such mechanisms seem to be more potent in the case of the ACF-EDP composites due to their larger active surface area (Table 3) and the uniform distribution of small spherical TiO₂ nanoparticles on the fiber surface (Figure 1d). These attributes likely favor the adsorption of phenol molecules and the activation of photocatalysis to a greater extent in comparison to the ACF-TTIP and ACF-P25 composites.

The activation of TiO₂ photocatalysts can also be explained through the UV spectra (190 to 390 nm) of samples collected during the experiments. According to Figure 5, significant variations in UV absorbance were observed throughout the wavelength range with treatment time. Specifically, a smooth sharp decay and shifting of the first characteristic peak at 205 nm to lower wavelengths are observed. Moreover, with increasing photocatalysis time, the main peak at 270 nm tends to decay, exhibiting several small peaks of gradually reduced absorbance. These trends are more pronounced in the case of the ACF-TTIP and ACF-EDP composites, thus providing additional support to the above findings.

The combined effect of adsorption and photocatalysis on phenol removal is also reflected in the kinetic analysis of the experimental data (Table 4). In particular, the rate of phenol removal may follow multiple-order kinetics. In the case of ACF-TTIP samples, phenol removal can be satisfactorily described by first-order kinetic equations, while the results obtained with the ACF-P25 and ACF-EDP samples are best fitted by second-order kinetic equations. Among the nine ACF/TiO₂ composite adsorbents, ACF-P25-30 and ACF-EDP-30 exhibit the greatest k_1 and k_2 kinetic constants, respectively. Variations in phenol removal rate are apparently associated with the differences in the adsorption and catalytic activity of each sample. Specifically, the exponential reduction of phenol (second-order kinetics) can be attributed mainly to the hydrophobic interactions of ACF fibers with phenol molecules,

whereas the direct dependence of phenol removal on the amount of TiO₂ immobilized on the carbon fiber (ACF-TTIP) is linked with first-order kinetics. These findings lead to the conclusion that the mechanism of phenol likely consists of two steps that are dynamic and dependent on the load and the morphology of the TiO₂ nanostructures on the fiber surface: (1) adsorption of phenol molecules on the surface of ACF/TiO₂; (2) surface photodegradation of phenol. The desorption of degradation products from the surface of the composite adsorbent is also possible; however, this is unclear in the present data, as the UV spectra (Figure 5) show an almost total disappearance of aromaticity from the treated solution (zero absorbance at wavelengths 250–280 nm).

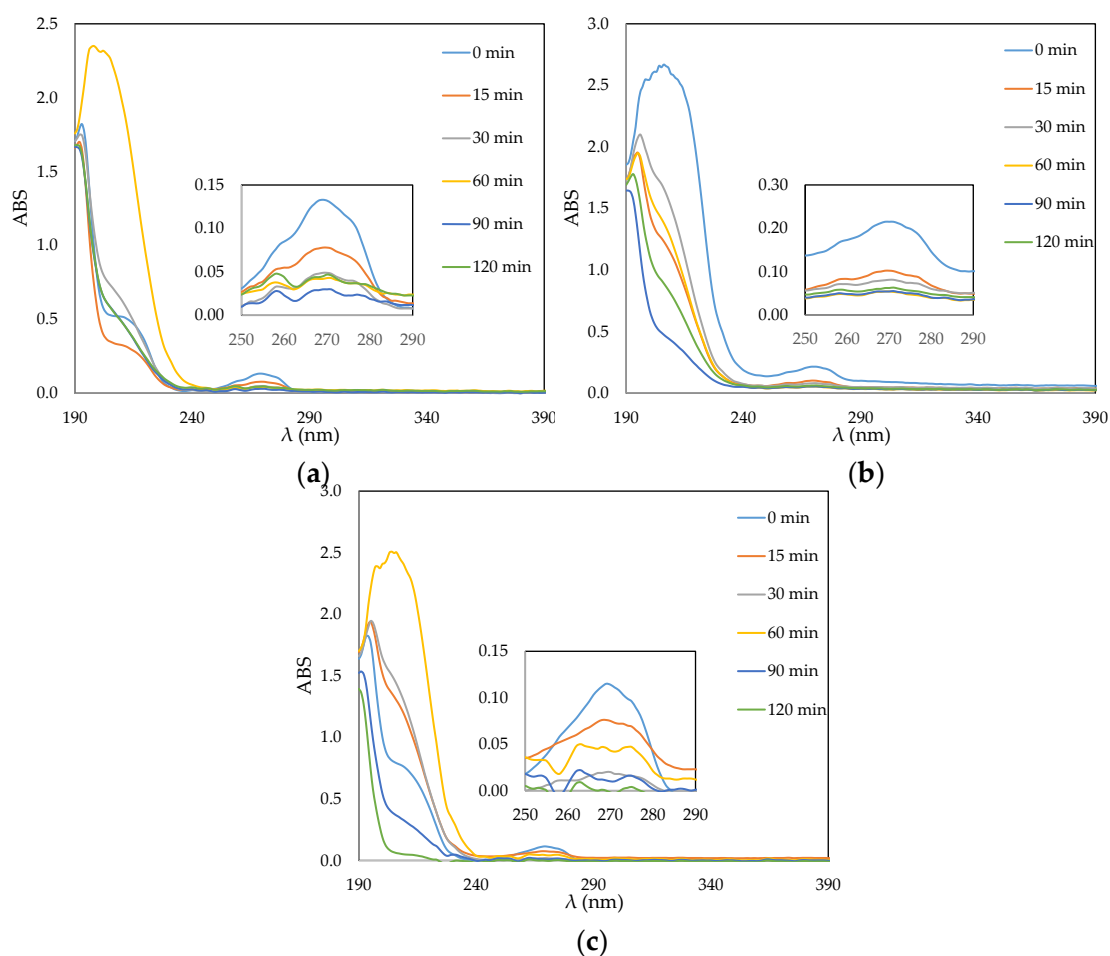


Figure 5. UV-Vis spectra of samples collected after 120 min of photocatalysis with the (a) ACF-TTIP-60, (b) ACF-P25-30, and (c) ACF-EDP-30 composite adsorbents.

Table 4. Kinetic analysis of phenol photocatalytic degradation experiments.

Sample	Zero Order		1st Order		2nd Order	
	k_0 (min ⁻¹)	R ²	k_1 (min ⁻¹)	R ²	k_2 (L mg ⁻¹ min ⁻¹)	R ²
ACF-TTIP-10	0.0599	0.8950	0.0098	0.9000	0.0017	0.8948
ACF-TTIP-30	0.1084	0.9549	0.0304	0.9664	0.0113	0.8319
ACF-TTIP-60	0.1175	0.9680	0.0123	0.9702	0.0015	0.9664
ACF-P25-10	0.0080	0.9651	0.0010	0.9730	0.0001	0.9776
ACF-P25-30	0.1537	0.7632	0.0370	0.9124	0.0115	0.9966
ACF-P25-60	0.0594	0.6865	0.0112	0.8149	0.0024	0.9256
ACF-EDP-30	0.0015	0.8929	0.0293	0.7812	0.0194	0.8493
ACF-EDP-60	0.0087	0.6985	0.0244	0.8637	0.0113	0.9365
ACF-EDP-120	0.0127	0.5192	0.0131	0.6476	0.0045	0.7946

The stability of the photocatalytic performance was examined in the case of the composite adsorbent that presented the most promising results (ACF-EDP-30). Table 5 shows the results of three cycles of phenol treatment by the same ACF-EDP-30 specimen. Each cycle consisted of two steps: (1) photocatalytic treatment of a 10 mg L⁻¹ phenol solution for 120 min; (2) regeneration of the composite adsorbent by applying UV irradiation for 120 min in a Milli-Q water solution. Results confirmed the successful regeneration of the composite photocatalyst and its steady performance, thus justifying the expectation of a prolonged service life of the synthesized ACF/TiO₂ composite by the electrophoretic method, which is a key issue for practical applications.

Table 5. Effect of repeated use on photocatalytic activity of ACF-EDP-30 composite adsorbent.

No of cycle	1	2	3
Phenol removal (%)	92.7	93.7	90.4

4. Conclusions

This study demonstrates the attributes of ACF/TiO₂ composite adsorbents, prepared by an electrophoretic coating method, for the removal of organic pollutants from water. SEM and BET analyses showed that TiO₂ coating on the ACF/TiO₂ composite adsorbents may negatively affect the adsorption capacity of the original ACFs, but it can still play an important role in the treatment of water by combined adsorption and photocatalysis. Experiments with phenol as a model organic pollutant shows that the removal efficiency is inversely proportional to the time of TiO₂ electrodeposition. The application of short electrophoresis times seems to favor the uniform distribution of TiO₂ nanostructures on the surface of the activated carbon fibers, which facilitates the rapid removal of phenol by a combined adsorption-photocatalysis mechanism. This behavior, along with the stable performance of the composite adsorbent prepared with electrophoresis in multiple cycles, provides evidence of the great potential of such materials for practical photocatalytic process applications. Ongoing research and development is aimed at material optimization and testing of the optimum photocatalytic adsorbent as anodic electrode in photo-electro-catalytic oxidation studies.

Author Contributions: Conceptualization, K.V.P.; methodology, K.V.P.; validation, K.V.P.; experimental investigation, A.T.; data interpretation, K.V.P. and A.J.K.; draft material preparation, writing—original draft preparation, K.V.P.; writing—review and editing, K.V.P. and A.J.K.; supervision, K.V.P. and A.J.K.; validation, K.V.P.; visualization, K.V.P. and A.T.; project administration, K.V.P. and A.J.K.; funding acquisition, K.V.P. and A.J.K.

Funding: This research has been co-financed by the European Regional Development Fund of the European Union and Greek national funds through the Operational Program Competitiveness, Entrepreneurship and Innovation, under the call RESEARCH-CREATE-INNOVATE (project code: T1EDK-04456).

Acknowledgments: The authors wish to thank SO-EN Co. Ltd. (Japan) for donating the activated carbon fiber (ACF) felt, as well as the personnel of Analytical Services Unit of the Chemical Process and Energy Resources Institute (ASU, CPERI) for analytical support.

Conflicts of Interest: The authors declare no conflict of interest. The funders had no role in the design of the study; in the collection, analyses, or interpretation of data; in the writing of the manuscript, or in the decision to publish the results.

References

1. Miklos, D.B.; Remy, C.; Jekel, M.; Linden, K.G.; Drewes, J.E.; Hübner, U. Evaluation of advanced oxidation processes for water and wastewater treatment—A critical review. *Water Res.* **2018**, *139*, 118–131. [[CrossRef](#)] [[PubMed](#)]
2. Giannakis, S.; Voumard, M.; Grandjean, D.; Magnet, A.; De Alencastro, L.F.; Pulgarin, C. Micropollutant degradation, bacterial inactivation and regrowth risk in wastewater effluents: Influence of the secondary (pre)treatment on the efficiency of Advanced Oxidation Processes. *Water Res.* **2016**, *102*, 505–515. [[CrossRef](#)] [[PubMed](#)]

3. Antonopoulou, M.; Evgenidou, E.; Lambropoulou, D.; Konstantinou, I. A review on advanced oxidation processes for the removal of taste and odor compounds from aqueous media. *Water Res.* **2014**, *53*, 215–234. [[CrossRef](#)] [[PubMed](#)]
4. Wang, J.L.; Xu, L.J. Advanced oxidation processes for wastewater treatment: Formation of hydroxyl radical and application. *Crit. Rev. Environ. Sci. Technol.* **2012**, *42*, 251–325. [[CrossRef](#)]
5. Andreatti, R.; Caprio, V.; Insola, A.; Marotta, R. Advanced oxidation processes (AOP) for water purification and recovery. *Catal. Today* **1999**, *53*, 51–59. [[CrossRef](#)]
6. Oturan, M.A.; Aaron, J.-J. Advanced oxidation processes in water/wastewater treatment: Principles and applications. A review. *Crit. Rev. Environ. Sci. Technol.* **2014**, *44*, 2577–2641. [[CrossRef](#)]
7. Mills, A.; Le Hunte, S. An overview of semiconductor photocatalysis. *J. Photochem. Photobiol. A* **1997**, *108*, 1–35. [[CrossRef](#)]
8. Chong, M.N.; Jin, B.; Chow, C.W.K.; Saint, C. Recent developments in photocatalytic water treatment technology: A review. *Water Res.* **2010**, *44*, 2997–3027. [[CrossRef](#)]
9. Karabelas, A.J.; Plakas, K.V.; Sarasidis, V.C. How far are we from large scale PMR applications. In *Current Trends and Future Developments on (Bio-) Membranes: Renewable Energy Integrated with Membrane Operations*, 1st ed.; Mozia, S., Molinari, R., Basile, A., Eds.; Elsevier Inc.: Amsterdam, The Netherlands, 2018; pp. 233–295.
10. Yahya, N.; Aziz, F.; Jamaludin, N.A.; Mutalib, M.A.; Ismail, A.F.; Salleh, W.N.W.; Jaafar, J.; Yusof, N.; Ludin, N.A. A review of integrated photocatalyst adsorbents for wastewater treatment. *J. Environ. Chem. Eng.* **2018**, *6*, 7411–7425. [[CrossRef](#)]
11. Suárez-García, F.; Martínez-Alonso, A.; Tascón, J.M.D. Activated carbon fibers from NOMEX by chemical activation with phosphoric acid. *Carbon* **2004**, *42*, 1419–1426.
12. Rabbi, A.; Dadashian, F. Simultaneous improvement in tensile strength and adsorption capacity of activated carbon fibers during stabilization and activation of acrylic fibers. *Diam. Relat. Mater.* **2019**, *95*, 174–184. [[CrossRef](#)]
13. Hou, Y.; Qu, J.; Zhao, X.; Lei, P.; Wan, D.; Huang, C.P. Electro-photocatalytic degradation of acid orange II using a novel TiO₂/ACF photoanode. *Sci. Total. Environ.* **2009**, *407*, 2431–2439. [[CrossRef](#)] [[PubMed](#)]
14. Sharma, A.; Lee, B.-K. Growth of TiO₂ nano-wall on activated carbon fibers for enhancing the photocatalytic oxidation of benzene in aqueous phase. *Catal. Today* **2017**, *287*, 113–121. [[CrossRef](#)]
15. Ao, C.H.; Lee, S.C. Enhancement effect of TiO₂ immobilized on activated carbon filter for the photodegradation of pollutants at typical indoor air level. *Appl. Catal. B Environ.* **2003**, *44*, 191–205. [[CrossRef](#)]
16. Nakata, K.; Fujishima, A. TiO₂ photocatalysis: Design and applications. *J. Photochem. Photobiol. C* **2012**, *13*, 169–189. [[CrossRef](#)]
17. Foo, K.Y.; Hameed, B.H. Decontamination of textile wastewater via TiO₂/activated carbon composite materials. *Adv. Colloid Interface Sci.* **2010**, *159*, 130–143. [[CrossRef](#)] [[PubMed](#)]
18. Wang, H.; Huang, X.; Li, W.; Gao, J.; Xue, H.; Li, R.K.Y.; Mai, Y.-W. TiO₂ nanoparticle decorated carbon nanofibers for removal of organic dyes. *Colloid Surf. A* **2018**, *549*, 205–211. [[CrossRef](#)]
19. Lazar, M.A.; Varghese, S.; Nair, S.S. Photocatalytic water treatment by titanium dioxide: Recent updates. *Catalysts* **2012**, *2*, 572–601. [[CrossRef](#)]
20. Reza, K.M.; Kurny, A.S.W.; Gulshan, F. Parameters affecting the photocatalytic degradation of dyes using TiO₂: A review. *Appl. Water Sci.* **2017**, *7*, 1569–1578. [[CrossRef](#)]
21. Riegel, G.; Bolton, J.R. Photocatalytic efficiency variability in TiO₂ particles. *J. Phys. Chem.* **1995**, *99*, 4215–4224. [[CrossRef](#)]
22. Stafford, U.; Gray, K.A.; Kamat, P.V.; Varma, A. An in situ diffuse reflectance FTIR investigation of photocatalytic degradation of 4-chlorophenol on a TiO₂ powder surface. *Chem. Phys. Lett.* **1993**, *205*, 55–61. [[CrossRef](#)]
23. Byrne, J.A.; Eggins, B.R.; Brown, N.M.D.; McKinney, B.; Rouse, M. Immobilisation of TiO₂ powder for the treatment of polluted water. *Appl. Catal. B Environ.* **1998**, *17*, 25–36. [[CrossRef](#)]
24. Pereira, L.A.; Couto, A.B.; de Lima Almeida, D.A.; Ferreira, N.G. The influence of TiO₂ amount on the photoactivity response for the novel TiO₂/BDD/carbon fiber ternary composite. *Diam. Relat. Mater.* **2017**, *75*, 18–24. [[CrossRef](#)]
25. Shi, J.; Zheng, J.; Wu, P.; Ji, X. Immobilization of TiO₂ films on activated carbon fiber and their photocatalytic degradation properties for dye compounds with different molecular size. *Catal. Commun.* **2008**, *9*, 1846–1850. [[CrossRef](#)]

26. Yao, S.; Li, J.; Shi, Z. Immobilization of TiO₂ nanoparticles on activated carbon fiber and its photodegradation performance for organic pollutants. *Particuology* **2010**, *8*, 272–278. [[CrossRef](#)]
27. Zhu, Y.; Fu, Y.; Ni, Q.-Q. Preparation and performance of photocatalytic TiO₂ immobilized on palladium-doped carbon fibers. *Appl. Surf. Sci.* **2011**, *257*, 2275–2280. [[CrossRef](#)]
28. Wang, C.; Yue, R.; Wang, H.; Zou, C.; Du, J.; Jiang, F.; Du, Y.; Yang, P.; Wang, C. Dendritic Ag@Pt core-shell catalyst modified with reduced graphene oxide and titanium dioxide: Fabrication, characterization, and its photo-electrocatalytic performance. *Int. J. Hydrog. Energy* **2014**, *39*, 5764–5771. [[CrossRef](#)]
29. Wang, Z.; Yoshinaga, K.; Bu, X.R.; Zhang, M. Low temperature fabrication & photocatalytic activity of carbon fiber-supported TiO₂ with different phase compositions. *J. Hazard. Mater.* **2015**, *290*, 134–141.
30. Hu, H.; Pang, B.; Zhu, Y.; Fu, Y. Preparation of titanium dioxide immobilized on carbon fibers annealed in steam ambient and their photocatalytic properties. *Text. Res. J.* **2017**, *87*, 2233–2241. [[CrossRef](#)]
31. Yu, H.; Quan, X.; Chen, S.; Zhao, H. TiO₂-multiwalled carbon nanotube heterojunction arrays and their charge separation capability. *J. Phys. Chem. C* **2007**, *111*, 12987–12991. [[CrossRef](#)]



© 2019 by the authors. Licensee MDPI, Basel, Switzerland. This article is an open access article distributed under the terms and conditions of the Creative Commons Attribution (CC BY) license (<http://creativecommons.org/licenses/by/4.0/>).